Received: 9 February 2019 | Revised: 18 November 2019 | Accepted: 20 January 2020

DOI: 10.1002/tal.1719

RESEARCH ARTICLE

WILEY

# Seismic retrofit design and risk assessment of an irregular thermal power plant building

Jianze Wang[1,2] | Kaoshan Dai[1,3,4] | Bowei Li[5] | Bo Li[1] | Yang Liu[1] | Zhu Mei[1] | Yexian Yin[6] | Jiahong Li[7]

[1]Department of Civil Engineering and Institute for Disaster Management and Reconstruction, Sichuan University, Chengdu, China

[2]Department of Disaster Mitigation for Structures, Tongji University, Shanghai, China

[3]Key Laboratory of Deep Underground Science and Engineering, Ministry of Education, Sichuan University, Chengdu, China

[4]Failure Mechanics & Engineering Disaster Prevention and Mitigation, Key Laboratory of Sichan Province, Sichuan University, Chengdu, China

[5]Department of Civil and Environmental Engineering, University of Michigan, Ann Arbor, Michigan

[6]SEPCOIII Electric Power Construction Corporation, Qingdao, China

[7]Hongrui Electric Power Engineering Consulting Co., Qingdao, China

**Correspondence**
Kaoshan Dai, Key Laboratory of Deep Underground Science and Engineering, Ministry of Education, Sichuan University, Chengdu, China.
Email: kdai@scu.edu.cn

**Funding information**
China Scholarship Council; Fundamental Research Funds for Central Universities of China; National Natural Science Foundation of China, Grant/Award Numbers: 51878426, U1710111; Program of Science and Technology Commission of Sichuan Province, Grant/Award Number: 18GJHZ0111; Power Construction Corporation of China, Grant/Award Number: KJ-2016-095

## Summary

Electric power system is one of essential lifeline systems for an urban community. An actual power plant building with typical coal-fired power generation process is selected to be studied in this paper. The detrimental impacts on the seismic performance of the structural system induced by heavy coal bunkers and irregular bracing configurations are expected to be mitigated by using retrofit strategies. A total of three retrofit design schemes that employ the isolation and supplemental damping techniques are developed. The original design scheme of the actual thermal power plant building that adopts steel special concentrically braced frame as lateral-force resisting system is used as benchmark for comparison purposes. Nonlinear response-history analyses are performed, and the obtained seismic responses are compared. To better quantify the benefit of the considered retrofit strategies, seismic risk in terms of probabilities of exceeding designated damage states as well as the downtime are analyzed. For the studied thermal power plant building, the results show that the added damping system is more effective in seismic risk reduction than the isolation for heavy coal bunkers. Compared to the original structural system design, the use of supplemental damping system cut the downtime of the thermal power plant building at most 42%.

**KEYWORDS**

damper, industrial building, irregular structure, isolation, retrofit design, seismic risk

## 1 | INTRODUCTION

Earthquake, as a destructive natural disaster, needs to be considered into the structural design of industrial plant buildings. The reconnaissance reports for recent seismic events such as Bam earthquake in 2003,[1] Chile earthquake in 2010,[2] Great East Japan earthquake in 2011,[3] and Emila earthquake in 2012[4] pointed out the high vulnerability of industrial plants would cause life threatening, economical losses, and environmental contamination after the earthquakes. Seismic damages were observed both in structural and nonstructural components such as column

  

supports, girders, mechanical equipment, piping systems, and storage racks. The resulting consequences ranged from the complete collapse to temporarily shut down and included a high likelihood of triggering uncontrolled fires and possible environmental damage.[5] Electric power system is an essential part in an urban community. Nowadays, the majority of global electricity generation is using fossil fuels.[6] Coal-fired thermal power plant is one of the most commonly used power plants and providing 40% of the world's electricity, especially in developing countries.[7] The functional interruption of a power plant due to earthquake disasters would result in immense economic and social loss to its associated urban regions.

Currently, common routines for seismic design of industrial buildings still follow conventional building design codes such as ASCE/SEI 7-10[8] and Eurocode 8.[9] Similar to residential building structures, the industrial building design is performed with the basic objective of to prevent building collapse under the maximum considered earthquake (MCE). In fact, as the thermal power plant is a part of the urban power generation system, a more stringent objective of continuous operation after moderate and small earthquake, is required. It can be achieved by elevating risk level in structural design and subsequently enlarging seismic demands in mandatory. As such, Chilean Ministry of Housing recently revised the design procedure for industrial buildings (i.e., NCh 2369)[10] with an intention to guarantee the continuous functionality of steel industrial structures even if the earthquake loading is sever than design-based earthquake intensity. However, recent earthquakes (e.g., Chile in 2010; Emila earthquake in 2012) have demonstrated that although buildings that were designed based on conventional seismic provisions endured minimal structural damage by earthquakes, they were still nonoperational because of extensive nonstructural damage.[2,4]

Nowadays, the performance-based design theory is widely developed and studied with the purpose to provide engineers and stakeholders with informed and quantified descriptions of consequences for decision making. The performance-based design basically entails the integration of seismic hazard, seismic demand estimation, fragility development, and loss estimation. Compared to the conventional design methods with limited basic objectives, the performance-based design theory enables practical engineers to set more specific design objectives and evaluate the design results in terms of repair cost, operational downtime, and life safety. In the past years, plenty of studies regarding performance-based structural design were performed. For example, Ellingwood[11] proposed a seismic risk assessment framework and applied it to steel and reinforced concrete frames. Rojas et al.[12] provided an automated performance-based design methodology to optimize the performance of structural and nonstructural systems of regular steel buildings in terms of social loss. Similarly, Hwang and Lignos[13] estimated the earthquake-induced loss of steel frame buildings by using a building-specific loss estimation methodology developed by Ramirez and Miranda.[14] In addition, the performance-based design theory was applied to innovative structural systems like self-centering moment frame[15] and buildings equipped with damping systems.[16,17] Tafakori et al.[18] performed risk-based retrofit design on an existing tall steel building. And eight retrofit alternatives were compared in terms of seismic risk and annual loss. Similarly, cost-benefit analyses were conducted by Liel and Deierlein[19] with the purpose to assess retrofit strategies on nonductile concrete frames. Han et al.[20] studied the benefit of using isolation technique on nonductile concrete buildings against the economic cost and indirect losses due to downtime and fatalities were also considered. It is worth noting that most previous studies focused on civil constructions, and few studies extended the use of performance-based design method to industrial buildings.

Since lessons from past earthquake events confirmed the devastating impact on industrial facilities, in order to improve the seismic resilience and prevent consequent accidents, some researchers applied seismic mitigation strategies to the industrial buildings. For example, Colombo and Almazán[21] assessed the influence of energy dissipation systems on the seismic damage of cylindrical steel tanks. Kanyilmaz and Castiglioni[22] performed incremental dynamic analyses to assess the merits of base isolations in industrial steel silos. The simulation results showed that the base isolations reduced the story drift demands as well as the collapse risk under strong earthquakes. Similarly, Rossi et al.[5] introduced friction pendulum isolators at the top of columns of supporting silos, and they found that the use of isolations eliminated the torsional effect and protected steel braces from buckling. In addition, a torsional hysteretic damping device was used into the retrofit design of existing silo structures in studies by Pinkawa et al.[23] The conducted incremental dynamic analysis results showed its effectiveness in preventing the global sideway collapse failure mode. Paolacci et al.[24] compared the efficiency of base isolation, energy dissipation devices, and traditional tuned-mass-damper device in seismic response reduction for chemical process plants by means of numerical simulations and physical tests. Noted that, most prior studies discussed the performance of seismic mitigation strategies in the aspect of structural behaviors and few built a link with the seismic risk.

In this study, an actual thermal power plant (TPP) building is considered. The seismic risk of the TPP building and the effectiveness of different seismic mitigation technologies in reducing the seismic risk are studied. At first, the performance-based retrofit design of the TPP building is performed. Unlike common residential buildings, the challenge of the design work is not only to properly communicate with the operational process but also consider how to protect the industrial equipment under earthquake loadings. One of the critical equipment, that is, coal bunker, is accounted into the lateral-force resisting system (LFRS) design of the TPP building. Subsequently, based on the complex structural topology of the building, the feasibility of the considered retrofit techniques in the TPP building is discussed. Following the modern building design provisions, a conventional LFRS system design and three retrofit system designs are developed. Nonlinear response-history analyses are conducted, and afterwards, seismic risks of all designed buildings are computed and compared. The effectiveness of the selected retrofit techniques is discussed. Finally, the contributions and limitations of the study are provided, followed by the conclusion section.

## 2 | A TYPICAL THERMAL POWER PLANT BUILDING

### 2.1 | Functional classification and structural configurations

In TPPs, the electric power is generated mainly by steam-driven turbines. In general, the power generation process includes several interconnected subsystems like steam and power generation system, coal conveyor system, coal crushing system, and feedwater system. The associated equipment and processing units of these subsystems are mostly placed in a single industrial building, which lead to the great importance of the building to the whole power plant. The typical configuration of the TPP building can be seen in in Figure 1. Based on the power generation process and equipment arrangement, the TPP building can be mainly divided into three parts: turbine hall, deaerator bay, and bunker bay.

The complex operational process raises plenty of constraints and limitations to structural design and consequently results in an irregular configuration for the TPP building. The structural typology of an actual TPP building considered in the current study can be seen in Figure 2. The building is generally 54.1 × 92 m in plan at the base. The spacing of frames along *X* direction is 10 m. The spans of turbine hall, deaerator bay, and bunker bay are 30.6, 10, and 13.5 m; the corresponding heights are 30.5, 38.4, and 53.3 m, respectively. The building also includes an extension at the north-east corner of the bunker bay (between Axis 01 and Axis 1) with a 6 m tall penthouse at the top. The lateral-force resisting system (LFRS) adopts concentrically braced frame, and the distribution of braced frames is indicated in Figure 2a. Also, Figure 2b,c shows the elevation views of the structure along *X* and *Y* directions, respectively. Each axis in *X* direction (i.e., Axes A, B, C, and D) has two braced frames that are between Axis 1 and Axis 2 and between Axis 9 and Axis 10. In contrast, it is noted that the operational process generates larger impact on the frame configuration in *Y* direction. Specifically, as seen from Figure 2b, the turbine hall is configured as a high-clearance warehouse, and the deaerator bay is designed as high-story moment frames so as to provide enough extension spaces for piping systems (Figure 1). The bunker bay is configured with chevron and inverted-chevron braces. With the intention of large-caliber pipelines and equipment freely cross the building, the first tier braced frame in bunker bay is designed with a "half" inverted-V type bracing. More specifically, there is only one brace member that connects the column base of Axis D to the middle of the girder on the first tier floor. Similarly, for the roof tier, a moment frame is used to resist lateral loadings instead. Another issue worth noting in the structural design of the TPP building is that there are seven coal bunkers shaped like silos installed at the 32.2-m level of the bunker bay. The coal bunkers are a vital part of the supply chain, and their loss of functionality may lead to business disruption of the whole TPP. For a common practice, the coal bunkers are rigidly connected to the girders by using 12-fixed supports. An illustration of the coal bunkers in the structural building can be seen in Figure 3. The seismic mass of each coal bunker, which is the sum of the weight of an empty bunker and the coal materials under normal service conditions is as much as 1,040 tons. Therefore, in seismic design especially for the structural part in bunker bay, a total of 7,280 (7 × 1,040) tons of mass at the 32.2-m level shall be considered. Such large mass concentration would impose detrimental effects on the seismic performance of the structure.[25]

### 2.2 | Resilient strategies for retrofit design of the TPP building

The resilience of a building structure can be enhanced by using isolation techniques, supplemental damping systems, or a combination of these.[18,26,27] By strategically using these techniques, structural repair and/or replacement of the added devices in the aftermath of an earthquake can be done in a short time. For the TPP building, suitable resilient strategies need to be selected to compromise with the corresponding

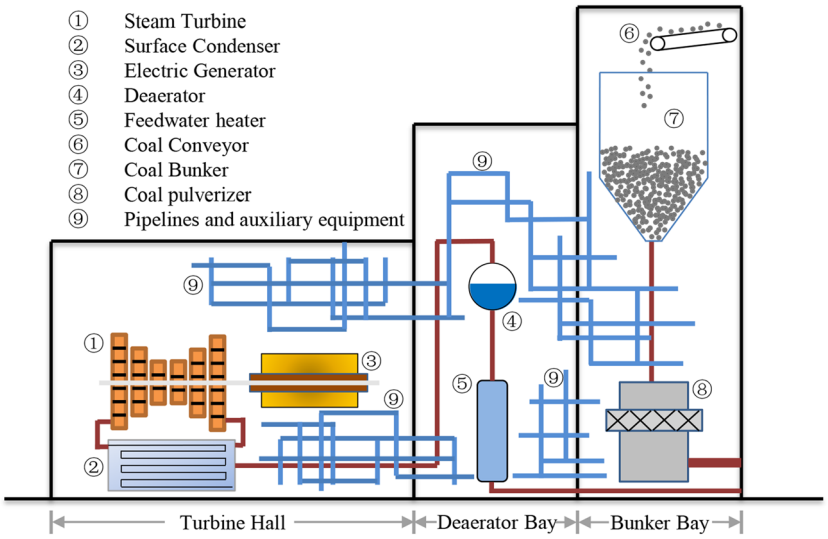


**FIGURE 1** Facility and equipment arrangement in the main industrial building of a typical power plant

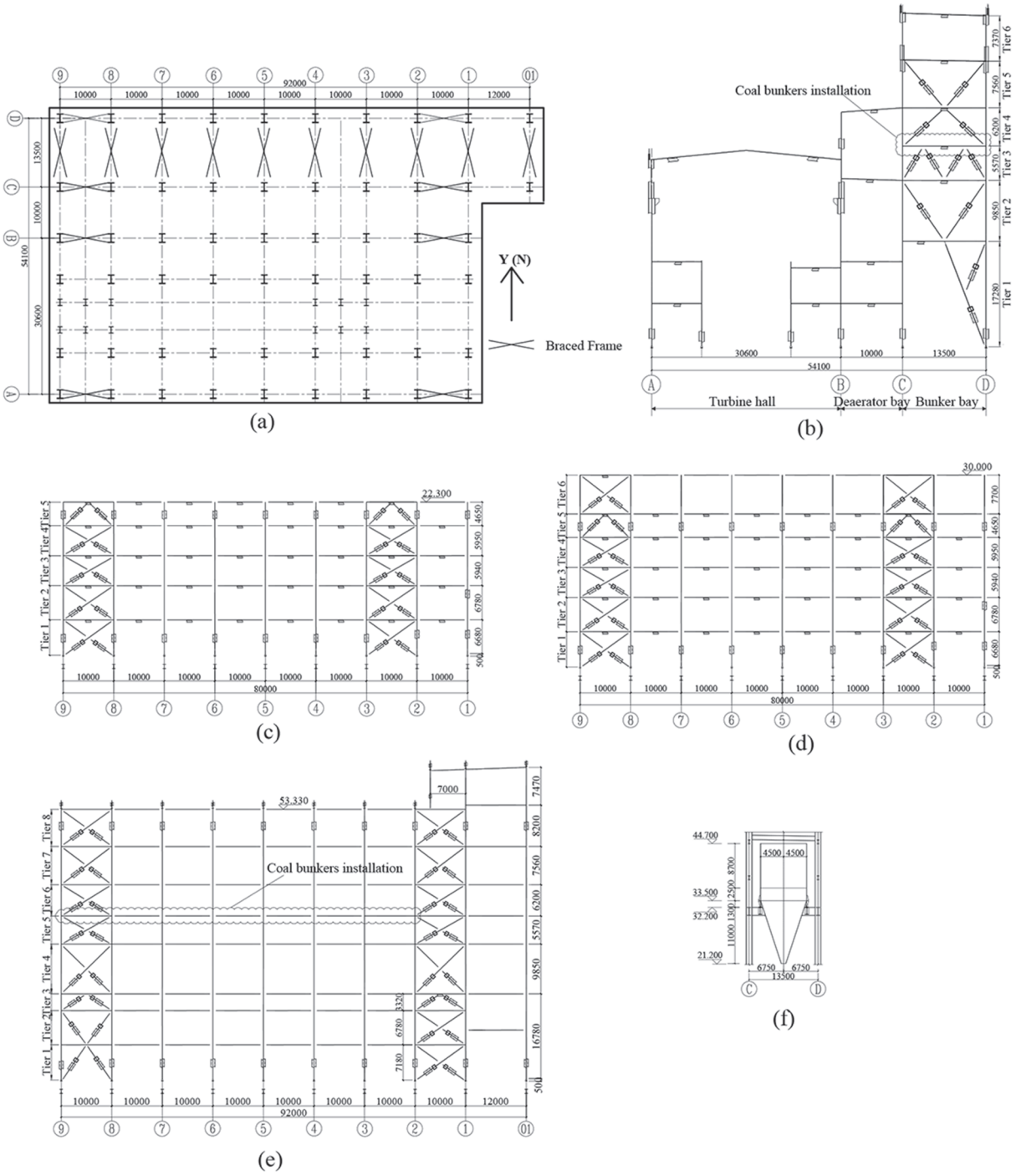


**FIGURE 2** A typical thermal power plan building considered in the study: (a) plan layout at the base, (b) elevation view along Axis 5, (c) elevation view along Axis A, (d) elevation view along Axis B, (e) elevation view along Axes C/D, and (f) elevation view of a single coal bunker

structural topology and operational constraints. Specifically, the large concentrated seismic mass (due to the existence of coal bunkers) and potential weak stories (due to discontinuous bracing systems) are of key interest to the retrofit design. Also, the damping system design (i.e., collections of damping devices and associated structural elements used to transfer forces from damping devices to LFRS[8]) is not allowed to interfere with the normal operational process. In other words, the supplemental damping systems are only permitted to be placed where the braced frames in the original structural system as shown in Figure 2a. Such constraint requires the damping system is capable to provide initial lateral stiffness and energy dissipations so as to avoid soft/weak stories due to sudden changes in lateral story stiffness/strength. Hence, metallic yield damping devices are preferred to be employed.

As indicated in prior studies, a significant contributor to total loss in special concentrically braced frame (SCBF) building systems is the repair cost for bracing components.[28] In addition, flexural buckling of steel braces typically occurs at a story ratio of approximately 0.5% in average,

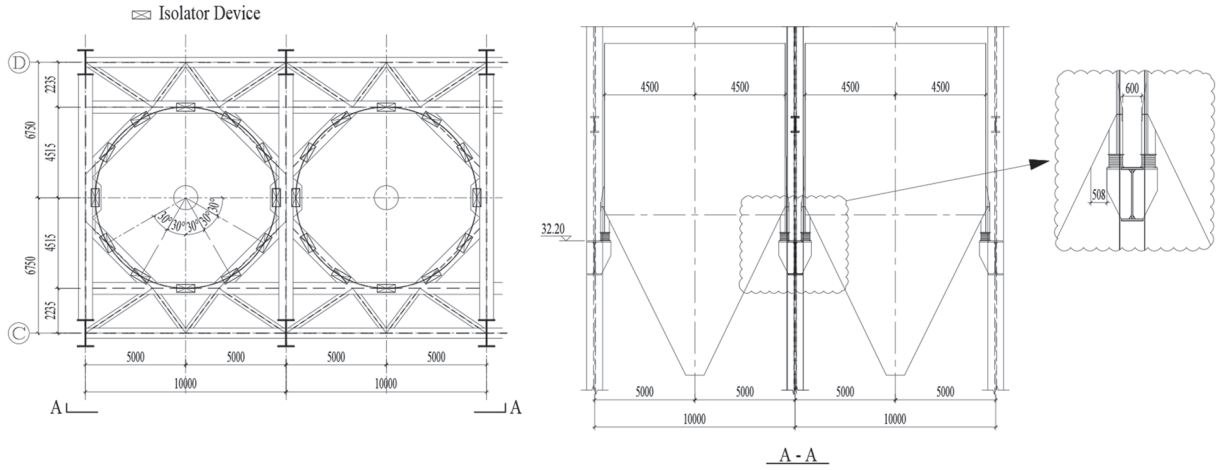


**FIGURE 3** Schematic illustration of coal bunker isolation

which may result in discontinuous operation of the TPP building under moderate earthquake loadings. Instead of the conventional hollow or wide-flange sectional bracing elements, buckling restrained braces (BRB) are first considered as an alternative because of their stable and consistent hysteretic behaviors in both tension and compression.[29] Another device considered in the retrofit design of the TPP building is the yielding shear panel device (YSPD), which dissipates energy by inelastic shear deformation of a low-yielding-point steel plate. As tested by previous studies, it has been demonstrated that the YSPD has a sound energy dissipation capacity and adequate elastic stiffness to withstand in-service lateral loadings (e.g., wind).[30]

As for the heavy coal bunkers installed at the level of 32.2 m, retrofit strategies are needed to reduce their adverse impact on the seismic demands of their supporting structural components. From past earthquake reconnaissance reports, similar storage silo-shaped facilities that commonly used in industrial structures caused severe damage even collapse to the supporting structural system.[31] Therefore, some researchers employed base isolations as a retrofit solution for existing industrial silo-type structures with an attempt to improve their seismic performance (e.g., Kanyilmaz & Castiglioni, 2017[22]; Fell et al., 2009[32]). As such, for the TPP building that are characterized by heavy coal bunkers, Dai et al.[33] introduced a partial mass isolation system and proposed a probabilistic-based design framework. The effectiveness of the isolation layers is optimized in terms of story-drift reduction with respect to a nonisolated structural system. In the following retrofit design for the TPP building, the isolation strategy is also considered specific for coal bunkers, and the associated isolator properties are determined using the method proposed by Dai et al.[33]

In sum, two resilient retrofit techniques—added damping system, which includes YSPD and BRB as well as isolation technique for coal bunkers are considered in this study. A total of three retrofit design schemes are developed: (a) Retrofit Design A: use of isolation system for coal bunkers; (b) Retrofit Design B: use of supplemental damping systems in LFRS design; and (c) Retrofit Design C: combined use of isolation and supplemental damping systems. The original structural system design is used as the baseline to compare against the three developed resilient structural systems.

## 3 | STRUCTURAL RETROFIT DESIGNS

The actual TPP building was originally designed according to the modern design codes AISC 360-10,[34] AISC 341-10,[35] and ASCE/SEI 7-10.[8] The design loads primarily include dead load, live load, wind load, and seismic load. The associated load combinations were performed in accordance with ASCE/SEI 7-10 standard. As shown in Figure 2, braced frames are placed in both principal structural axes. The design requirements related to SCBF system prescribed in AISC 341-10 are followed. The wide flange sections are adopted for columns and beams. The square hollow structural shapes (HSS) are used for brace members. The beam-column connections are welded, so fully restrained assumption is made in design analyses. The braces are connected to columns and beams through gusset plate connections, and each has an elliptical clearance of eight times the thickness of the gusset plate so as to accommodate brace-end rotation demands.[36] The strength (e.g., compression, flexure, and buckling) of every structural component as well as connections are examined in accordance with AISC 360-10.[34] The TPP building is actually located at a high seismic-prone zone in China with Site Class D. The corresponding mapped spectral acceleration parameters, that is, $S_s$ at short period and $S_1$ at a period of 1 s, are 1.4 and 0.9 g, respectively. As the TPP building is constructed as a kind of lifeline facilities, the Risk Category III and Seismic Design Category D are assigned. And hence, the importance factor $I$ = 1.25, response modification factor $R$ = 6, deflection amplification factor $C_d$ = 5.5, and overstrength factor $\Omega_0$ = 2.0 are considered in the original design of the LFRS for the TPP building.

### 3.1 | Retrofit Design A: Isolation system for coal bunkers

The first retrofit design only employed isolation technique specific for the heavy coal bunkers at the level of 32.2 m of the frame between Axis C and Axis D (i.e., bunker bay). Again, for a conventional practice, the coal bunker is rigidly connected to the girders by using 12 fixed supports. With the introduction of isolation strategy, the fixed supports are replaced by lead-rubber bearing (LRB) devices, and an illustration can be seen in Figure 3. The isolation layer that is composed of 12 isolator devices for each coal bunker is fabricated with a purpose to reduce the inertial motions of the heavy coal bunkers. The compression strength of the LRB isolator is ensured to have the ability to withstand the vertical loadings imparted by the connected coal bunker. The initial stiffness of the isolation layer is designed to be large enough to resist the serviceable loads such as wind loadings and lateral impact by falling of coal materials from the top conveyor. The effective stiffness of the isolator device is a key property to the performance of the entire isolation system. The idealized situation is where the movement mechanism of the isolated coal bunker is designed to work as a tuned mass damper. Therefore, the lower supporting structures are subjected to the antimotion force induced by the coal bunkers. Such design was achieved in another study of the authors.[33] The installation space in situ and allowable deformation should also be considered in the sizing of the isolator device. An isolator device available in business market is used, and the corresponding parameters are listed in Table 1. The allowable deformation of the isolation device is limited by the gap of two adjacent coal bunkers (i.e., 400 mm as seen in Figure 3) in case of pounding during an earthquake, also limited by the deformation capacity of the isolator (i.e., 385 mm). Based on the stiffness properties of the selected isolator and the seismic weight of a coal bunker, the natural period of a single isolated coal bunker is computed as 2.11 s.

### 3.2 | Retrofit Design B: Use of damping system in LRFS design

As discussed in Section 2.2, the YSPD and BRB devices are considered in the retrofit design. The Chapter 18 of ASCE/SEI 7-10 that details the requirements of structural design with added damping systems is followed. A value of 8% additional effective damping to the LFRS in each principle direction of the structure is set as the design objective. Although there have been proposed design methods for structures with supplemental dampers in prior studies, an iterative process for design objective achievement is inevitable.[37] Based on the original design scheme, an iterative design work that includes variations in properties of damping devices as well as their distribution is carried out with the help of SAP2000 V18.[38] The locations, numbers, and properties of damping systems are presented in Table 2. The initial stiffness of BRB device stands for the elastic stiffness of the steel yielding core, which is later used in the numerical modeling. The initial stiffness of YSPD is the average tangential stiffness of the steel plate before yielding, and the value of which is usually provided by the manufacture. The bracing elements that transfer forces from YSPD to the rest seismic structural members are designed to remain elastic under earthquake loadings in MCE intensity. The inverted *V*-configured and *X*-configured bracing systems are used for the YSPD connection (Figure 4a).

**TABLE 1** Parameters of isolator device for coal bunker isolation

| Outer bossunded rubber diameter (mm) | Initial stiffness, $K_0$ (kN/mm) | Postyield stiffness, $K_F$ (kN/mm) | Yielding strength, $F_Y$ (kN) | Vertical stiffness, $K_V$ (kN/mm) | Allowable deformation |
|---|---|---|---|---|---|
| 700 | 9.97 | 0.77 | 106 | 3,509 | 385 |

**TABLE 2** The arrangement of supplemental damping systems in Design B

| Frame | Tier number | Damping device | Quantity | Yielding strength (kN) | Initial stiffness (kN/mm) |
|---|---|---|---|---|---|
| Axes A and B | 1 | YSPD | 2 | 1,800 | 1,200 |
| | 2 | | 2 | 1,500 | 1,000 |
| | 3 | | 2 | 1,000 | 667 |
| Axes C and D | 2 | YSPD | 2 | 2,000 | 1,333 |
| | 3 | BRB | 4 | 2,500 | 1,250 |
| | 4 | | 4 | 3,000 | 1,500 |
| | 5 | YSPD | 2 | 1,800 | 1,200 |
| | 7 | YSPD | 2 | 1,200 | 800 |
| Axes 1 to 8 | 1 | BRB | 1 | 4,500 | 2,250 |
| | 2 | BRB | 1 | 4,500 | 2,250 |
| | 3 | YSPD | 2 | 1,200 | 800 |
| | 5 | YSPD | 1 | 1,200 | 800 |

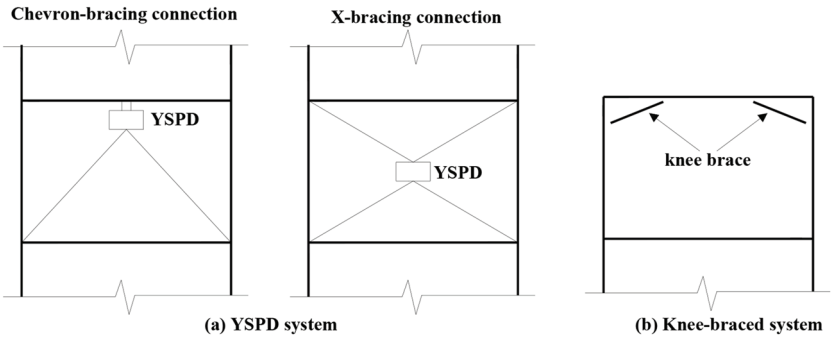


**FIGURE 4** Schematic illustration of utilized resilient strategies. YSPD, yielding shear panel device

It is also noted that the bracing system at the top two tiers of the *Y*-directional frames (Figure 2b) is discontinuous, which may lead to weak and soft tiers. The coal conveyor that is located at the sixth tier in the bunker bay (Figure 1) has to extent through the building along *X* direction (i.e., from Axis 01 to Axis 9). It is a part of the supply chain for coal material in the TPP building, and therefore, the structural damage in the sixth tier is expected to be reduced. However, supplemental damping systems such as diagonal BRB and YSPD together with V-type or X-type bracings are not allowed due to their architectural obstructions. Instead, the moment frame of sixth tier in the bunker bay is strengthened by using stocky knee braces, as presented in Figure 4b. The effectiveness of the knee-braced system has been investigated[39–41] by means of physical tests and numerical analyses. Using the design method provided by Leelataviwat et al.,[42] yielding and buckling damage initially occur at the knee braces and then followed by plastic hinging formation in the connected moment frame. The damaged knee brace can be repaired and/or replaced after an earthquake, which helps to facilitate the functional recovery and structural repair process.

### 3.3 | Retrofit Design C: Combined use of isolation and supplemental damping system

For the Retrofit Design C, both techniques of the isolation for coal bunkers and supplemental damping systems are utilized. Since the heavy coal bunkers are installed on the level of 32.2 m in bunker bay, the considered isolation strategy is likely to benefit the substructures below the coal bunkers only (i.e., first to fifth tiers for Axes C and D and first to third tiers for Axes 1 to 9 [Figure 2]). For the rest substructures (i.e., frames between Axis A and Axis B and frames above coal bunkers between Axis C and Axis D), the damping devices are added to reduce the corresponding seismic demands and structural damage.

With a comparison purpose, the properties of isolator devices for Retrofit Design C adopted those same with Retrofit Design A (Table 1). Considering the use of isolation for coal bunkers, the supplemental damping system is mandatorily prohibited for the structures below the coal bunkers which are specifically the frames between Axis C and Axis D. On the contrary, for frames in *Y* direction (i.e., Axis 1 to Axis 9), BRB devices are still considered for the first tier due to the unsymmetrical bracing configuration (Figure 2b). Analogous to the Retrofit Design B, the added damping systems are designed following the Chapter 18 of ASCE/SEI 7-10, and the design results are listed in Table 3. The knee-brace strategy is also employed for the roof tier in *Y*-directional frames.

## 4 | NUMERICAL MODELING

Recall that the original TPP building design as well as the three retrofit designs were examined using SAP2000 V18. The first three mode shapes of the original TPP building are presented in Figure 5. The first two modes follow translational motions patterns along the two principle directions of the building. And the third mode follows torsional motion around the vertical axis of the building. It is noted that due to the complex structural configuration of the TPP building, the effective mass ratios of the first and second translational modes are as much as 63% and 73%, respectively.

**TABLE 3** The arrangement of supplemental damping systems in Design C

| Frame | Tier number | Damping device | Quantity | Yielding strength (kN) | Initial stiffness (kN/mm) |
|---|---|---|---|---|---|
| Axes A and B | 2 | YSPD | 2 | 1,200 | 800 |
| | 3 | | 2 | 800 | 533 |
| Axes C and D | 6 | YSPD | 2 | 1,500 | 1,000 |
| Axes 1 to 8 | 1 | BRB | 1 | 4,500 | 2,250 |
| | 2 | BRB | 1 | 4,500 | 2,250 |

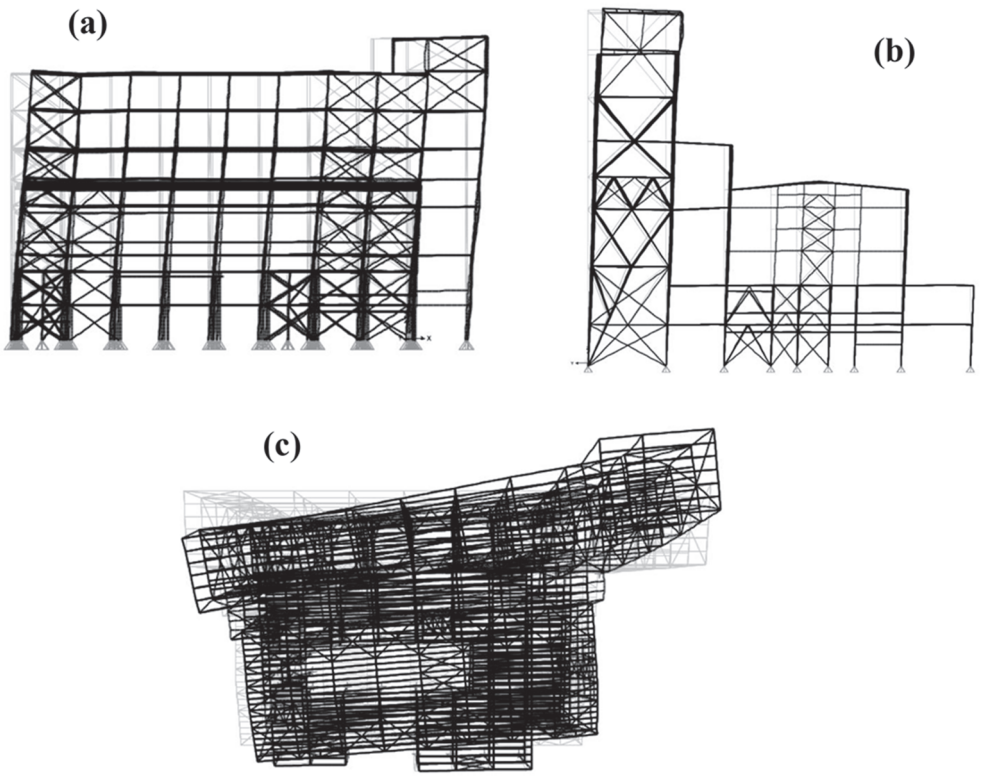


**FIGURE 5** Mode shapes: (a) Mode 1—translational motion along *X* direction; (b) Mode 2—translational motion along *Y* direction; and (c) Mode 3—torsional motion

And hence, a total of 60 modes were considered in dynamic analyses so that the accumulated modal mass participated in translational motions in each principle axis of the building is greater than 90%. The mode periods of the original design and three retrofit designs are compared in Table 4. It can be seen from the table that the dynamic properties of the four designed buildings are close. The obtained dynamic characteristics are also similar to the study result provided by Dai et al.,[33] which verifies the sufficiency of the developed numerical model.

Three-dimensional nonlinear structural models for all considered building designs are built using PERFORM-3D,[43] which enables the nonlinear response history analyses (RHAs) conducted with a sound efficiency and convergence. Every numerical model includes both the LFRS (i.e., braced frames) and the gravity framing system. The Rayleigh damping of 3% at $0.2T_1$ and $1.0T_1$, where $T_1$ is the fundamental period, is considered in RHAs. Also, a time step of 0.005 s is assigned to each loading case. Global *P*-Δ effect is directly incorporated in the analysis, and geometric nonlinearity is assigned to all structural elements. The nonlinear dynamic analyses are set to terminate when the solution fails to converge or when excessive roof drift ratio of 10% in the principal structural axes is reached. A 10-s duration of zero-amplitude acceleration time history is added at the end of each ground motion to identify the residual drift after the actual excitations.

The modeling techniques for structural components, isolators, and damping systems are verified and presented in detail in the following sections.

## 4.1 | Braced frame

As prescribed by AISC 341-10,[35] columns and beams in SCBF are designed as force-controlled components, and braces are designed as deformation-controlled components. In other words, columns and beams shall remain essentially elastic even under severe earthquake loading. Braces are expected to behave nonlinearly to dissipate energy. The potentiality of going into plastic for beams and columns are still considered in

**TABLE 4** Information of the first three modes of the TPP building

| Mode | Original design | Retrofit Design A | Retrofit Design B | Retrofit Design C |
|---|---|---|---|---|
| 1 | 2.00 | 2.04 | 1.95 | 1.97 |
| 2 | 1.50 | 1.62 | 1.30 | 1.33 |
| 3 | 0.84 | 1.12 | 1.08 | 1.11 |

numerical model, by assigning flexural nonlinear hinges at both ends of components. The backbone curve of the nonlinear hinge elements provided by PERFORM-3D[43] can be seen in Figure 6a. The required parameters such as $F_Y$, $F_R$, $a$, and $b$ are determined based on suggestions from ASCE/SEI 41-13.[44]

The buckling behaviors of braces are simulated by using the nonlinear steel bar/tie/strut element wrapped with buckling materials. Such nonlinear model follows an elastic perfectly plastic backbone in tension and a buckling relationship in compression. The corresponding backbone curve can be seen in Figure 6b. The stress values specified for Point A and Point B are assigned with 1% and 15% of tension strength, and the strain values are 45% and 50% of the strain range of the hysteresis loop, respectively. The stretch factor, which controls the tension stretch after an increased buckling deformation, is taken as the value of 0.75. The ductility ratio and residual strength (after strength deterioration) for braces in tension and in compression are obtained from stipulations in ASCE/SEI 41-13.[44] The parameter values mentioned above are verified by using the results from cyclic loading tests of a single-bay braced frame.[45] Figure 7 shows the comparison between the simulation and test results on the hysteretic loops of a brace element. A good agreement in the aspects of yielding/buckling strength and deteriorations in strength and stiffness is achieved as seen from the figure.

## 4.2 | Isolations for coal bunkers

The simulation of coal bunker was simplified by using body-constrained nodes, which include supporter nodes and a mass node located at the center of gravity of the entire coal bunker. A schematic view of the simplified model can be seen in Figure 8. The center of mass node (blue point in Figure 8) is assigned with the seismic mass of an entire coal bunker (i.e., 1,040 tons). The effectiveness of such simplified model for coal bunker was also studied by Pinkawa et al.[23] In this study, the fixed supporters for coal bunkers in the original design and Retrofit Design B are modeled using rigid links. For Retrofit Design A and Retrofit Design C (i.e., using isolations for coal bunkers), the isolator device is modeled by rubber-type seismic isolator element available in PERFORM-3D. The hysteric behavior of such element is basically described with a trilinear model (Figure 9a). The initial stiffness $K_O$, postyielding stiffness $K_F$, yielding strength $F_Y$, and allowable deformation $D_X$ are specified according to Table 2. Other parameters required in the model, specifically $F_U$ and $D_U$, are taken as 1.25 times the yielding strength and 3.75 times the yielding deformation,

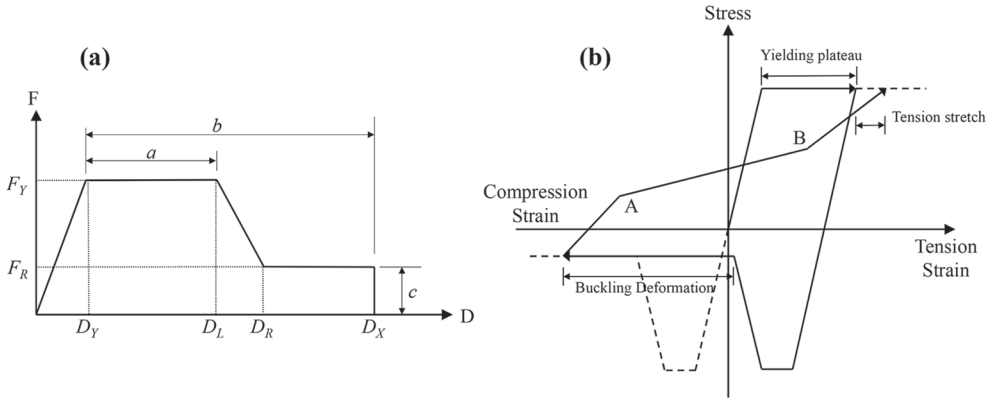


**FIGURE 6** Finite element models used for braced frame components: (a) backbone curve for nonlinear hinges and (b) hysteric model for brace elements[43]

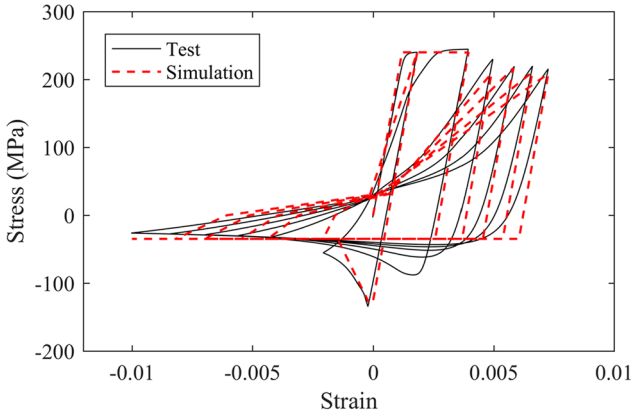


**FIGURE 7** Comparison of hysteretic behaviors of brace element between test result and numerical simulation

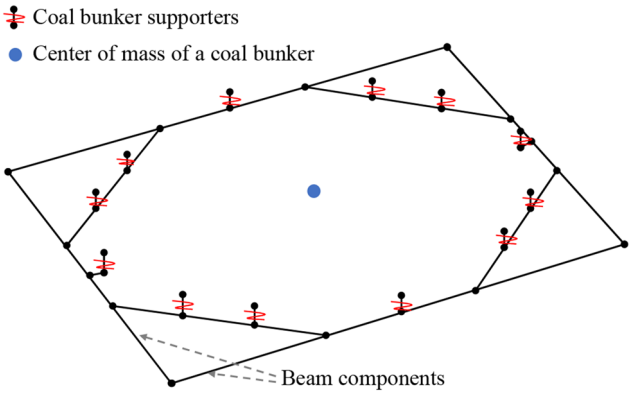


**FIGURE 8** Schematic view of coal bunker model

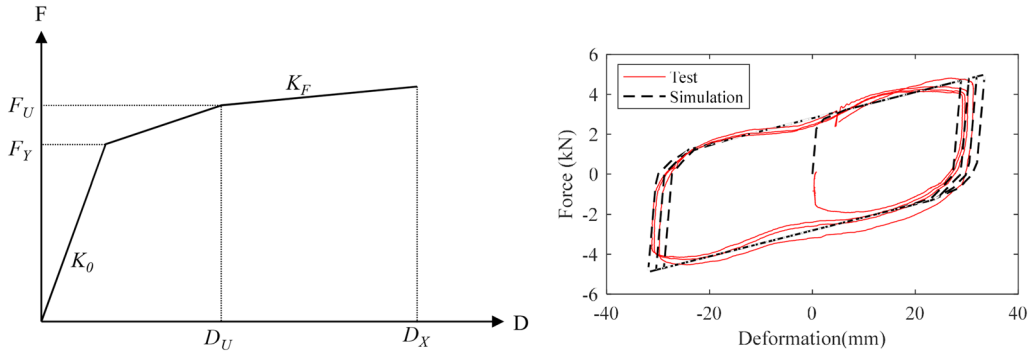


**FIGURE 9** Element model for isolator device

respectively. The parameter values as taken above are also verified based on a cyclic loading test result performed on a lead-rubber bearing device.[46] Figure 9b shows the comparison between the test and simulation result of an isolator device, and a good agreement is indicated from the figure.

## 4.3 | Modeling of YSPD device

The YSPD device was modeled using the shear-type infill panel element provided by PERFORM-3D,[43] which follows a trilinear force-deformation relationship as seen in Figure 10a. The parameters of initial stiffness $K_0$ and yielding strength $F_Y$ are determined based on Table 2 and Table 3 for Retrofit Design B and Retrofit Design C, respectively. The postyielding stiffness $K_H$ is taken as 18% of $K_0$. The ultimate strength $F_U$ and deformation $D_U$ are assigned with $1.17F_Y$ and $4.5D_Y$, respectively. The allowable deformation $D_X$ is taken as 10% height of the story where the YSPD is placed. The element model as well as the parameter values are verified by using a cyclic loading test result.[46] The comparison

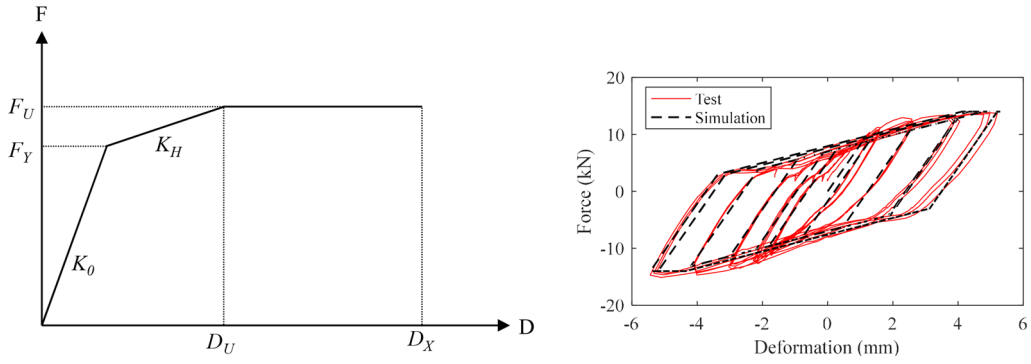


**FIGURE 10** Element model for YSPD device

between the test and simulation results is made in Figure 10b, and it shows that the considered element model is adequate to predict the hysteretic behaviors of the YSPD device.

### 4.4 | Modeling of BRB component

PERFORM-3D[43] provides a specific element for modeling BRB component, and the corresponding force-deformation relationship is shown in Figure 11a. The yielding strength and elastic stiffness of BRB components considered in the Retrofit Design B and Retrofit Design C are determined by the values indicated in Tables 2 and 3, respectively. The upper bilinear lines beyond $F_Y$ point in the model is to account for isotropic hardening effect, which induces increase in the component strength under cyclic loadings. In this study, the amount of strength increase is considered by selecting "maximum deformation only" in PERFORM-3D and specifying 2.0 for maximum deformation at $F_{U0}$–$F_{UH}$, 3.5 for maximum deformation at $F_{UH}$ as suggested by Speicher and Harris.[47] In addition, the values of $1.11F_Y$ and $1.67F_Y$ are considered for postyield strength $F_{U0}$ and $F_{UH}$, respectively. The parameter of deformation $D_U$ corresponding to $F_{U0}$ is taken as the 0.175% of the BRB component length. The value of 1.5% $K_0$ is specified for the postyield stiffness $K_F$. And the maximum deformation $D_X$ is determined by 6% of the BRB component length. Such modeling techniques and values of parameters are also verified based on test results performed on a BRB device under cyclic loadings.[46] Figure 11b compares the test and simulation results, and a good agreement validates the BRB element model as used in this study.

## 5 | SEISMIC RISK ANALYSIS

### 5.1 | Ground motion selection

The seismic performance assessment of the developed four design schemes of the TPP building incorporates nonlinear response-history analyses. An ensemble of 15 pair ground motions is selected from PEER NGA database[48] based on the acceleration response spectrum at the MCE intensity (i.e., with an exceedance probability of 2% in 50 years). The spectra of the selected ground motions at the SRSS ordinate as well as the target spectrum are plotted in Figure 12. The ground motions were selected with the criteria, which include moment magnitude ($M_w$) covers the range of 5.9–7.6; the source-to-site distance ($R_{rup}$) is within 22–198.1 km; the average shear velocity in 30 m upper soils ranges from 179 to 276 m/s. The ground motion scaling was done until the median spectrum has a less than 10% mean square error with respect to the target spectrum. The details of the selected ground motion are summarized in Table 5. To develop the seismic fragilities, nonlinear response-history analyses are performed at ground motion intensity levels ranging from 60% to 140% of MCE at 20% increment. Such range of ground motions covers the design-based earthquake (i.e., 67% of MCE), the 100% MCE, and the extremely rare earthquake incidents (i.e., greater than 100% of MCE). A total of 75 analyses are performed for each designed building.

### 5.2 | Seismic demand comparison

The seismic demands of the four considered designed structures are obtained from nonlinear response-history analyses. Figure 13 compares the roof drift time-history responses of all designed buildings under the ground motion recorded by Delta Station in Imperial Valley earthquake. There, it is clear from the figure that the original design has the largest value of peak roof drift in *X* direction (i.e., 0.47%), which is nearly two times the

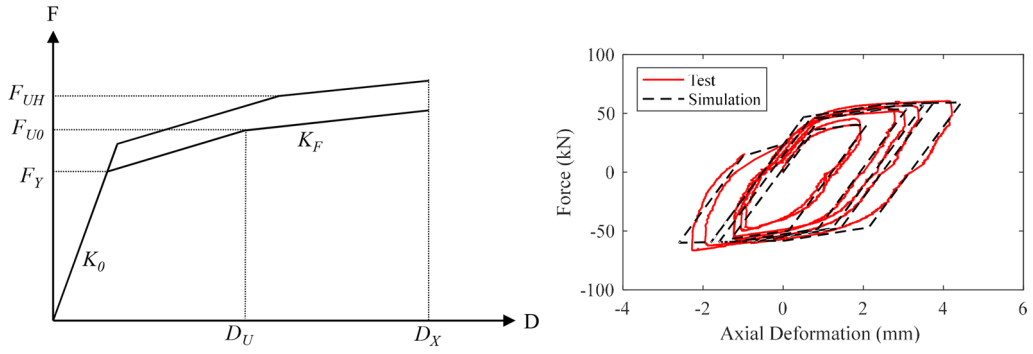


**FIGURE 11** Element model for BRB device

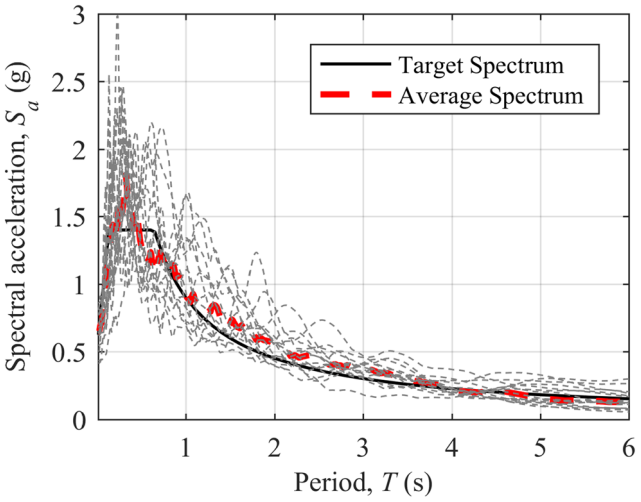


**FIGURE 12** Spectra of selected ground motions and the target spectrum

**TABLE 5** Summary of the selected ground motions

| No. | Earthquake name | Year | Station name | Mw | Rrup (km) | Vs30 (m/s) | MSE |
|---|---|---|---|---|---|---|---|
| 1 | Borrego | 1942 | El Centro Array #9 | 6.5 | 56.9 | 213.4 | 9.40% |
| 2 | El Alamo | 1956 | El Centro Array #9 | 6.8 | 121.7 | 213.4 | 8.21% |
| 3 | Friuli Italy-02 | 1976 | Codroipo | 5.9 | 41.4 | 249.3 | 6.67% |
| 4 | Imperial Valley-06 | 1979 | Calipatria Fire Station | 6.5 | 24.6 | 205.8 | 8.65% |
| 5 | Imperial Valley-06 | 1979 | Delta | 6.5 | 22.0 | 242.1 | 2.72% |
| 6 | Imperial Valley-06 | 1979 | El Centro Array #13 | 6.5 | 22.0 | 249.9 | 7.97% |
| 7 | Superstition Hills-02 | 1987 | Imperial Valley Wildlife Liquefaction Array | 6.5 | 23.9 | 179.0 | 7.73% |
| 8 | Loma Prieta | 1989 | Agnews State Hospital | 6.9 | 24.6 | 239.7 | 8.57% |
| 9 | Loma Prieta | 1989 | Dumbarton Bridge West End FF | 6.9 | 35.5 | 238.1 | 8.89% |
| 10 | Loma Prieta | 1989 | Hollister Differential Array | 6.9 | 24.8 | 215.5 | 5.56% |
| 11 | Taiwan SMART1(45) | 1986 | SMART1 I01 | 7.3 | 56.2 | 275.8 | 8.12% |
| 12 | Chi-Chi Taiwan | 1999 | CHY015 | 7.6 | 38.1 | 228.7 | 9.89% |
| 13 | Manjil Iran | 1990 | Rudsar | 7.4 | 64.5 | 242.1 | 9.42% |
| 14 | Hector Mine | 1999 | 12440 Imperial Hwy North Grn | 7.1 | 176.6 | 276.4 | 7.83% |
| 15 | Hector Mine | 1999 | Newhall - Fire Sta | 7.1 | 198.1 | 269.1 | 7.04% |

values observed from the Retrofit Design A and Retrofit Design C. The Retrofit Design B has the peak roof drift of 0.28% in *X* direction, which is slightly larger than the other two retrofit designs. As for peak roof drift response in *Y* direction, the considered four building designs have close results. But during the time of 20 to 40 s, the original design shows the largest response and followed by Retrofit Design A. In addition, the response histories of the Retrofit Design B and Retrofit Design C are almost the same. Noted that the comparison made in Figure 13 is the result under a single ground motion pair. A total of 75 analysis results for each designed building are statistically processed and discussed in the following.

Figures 14 and 15 show the distributions of peak tier drift ratios under 100% MCE excitations at the Axis A, Axis B, and Axis D frame columns in *X* direction and *Y* direction, respectively. For drift demands in *X* direction, the results of these four are close in some tiers such as the first two tiers in these three axis columns as well as the top tier in Axis D. For most of the rest tiers, Retrofit Design B has the smallest drift ratios. On the contrary, the original design has the largest drift ratios. The largest difference is observed for results of the fifth tier in Axis D where the coal bunkers are installed. The corresponding mean tier drift ratio at the fifth tier of the original design is greater than 2%. With the introduction of different retrofit strategies, the drift ratios for Retrofit Design A, Retrofit Design B, and Retrofit Design C are reduced to 1.54%, 1.10%, and 1.34%, respectively. As can be seen from Figure 15, all the four structures experienced smaller drift demands in *Y* direction than those in *X* direction. The largest drift in *Y* direction occurred at the first tier for every considered structure. The original design has the largest drift ratios at the first tier for both Axis A and Axis B frames, which are around 1.5%. Conversely, the Retrofit Design C has the best performance in *Y*-directional drift response, followed by the Retrofit Design B and Retrofit Design A. Taking the results of Axis A frame as an example, compared to the original design, the

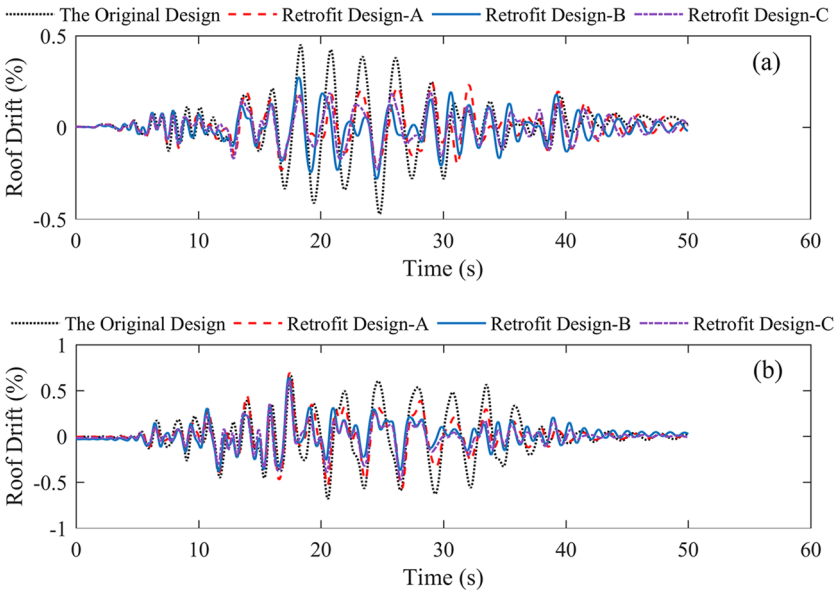


**FIGURE 13** Comparison of roof drift time-history response: (a) *X* direction; (b) *Y* direction

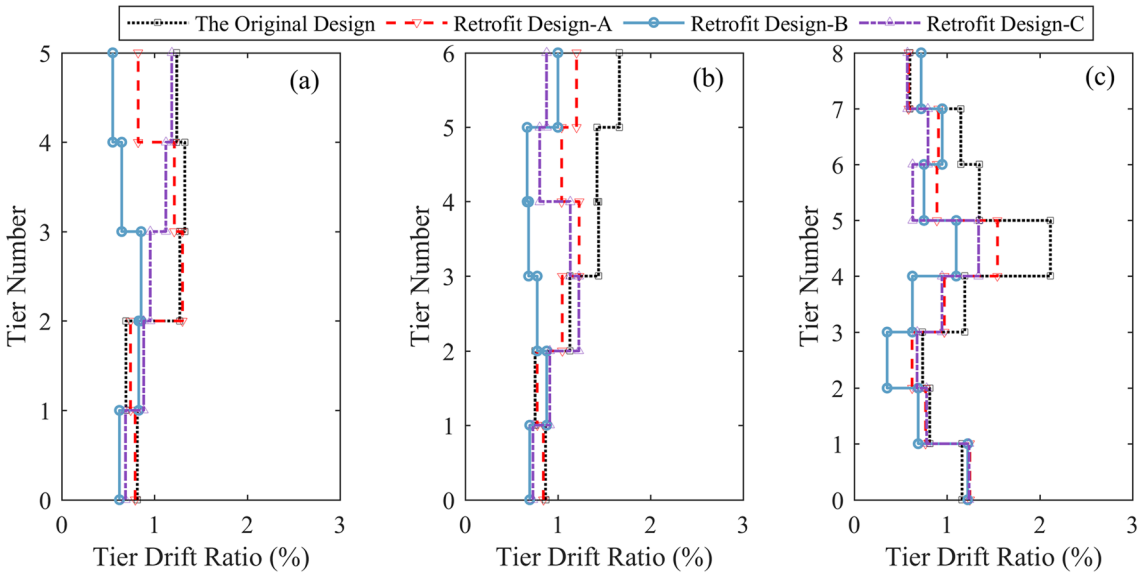


**FIGURE 14** Distributions of mean story drift ratios under 100% MCE in *X* direction for columns in (a) Axis A, (b) Axis B, and (c) Axis D

drifts of the first tier are reduced by 15%, 24%, and 33% for Retrofit Design A, Retrofit Design B, and Retrofit Design C, respectively. In general, it is clear from Figures 14 and 15 that the isolation of coal bunkers (i.e., Retrofit Design B) did reduce the drift demands not only in tiers that below the coal bunkers in Axis D frames but also in tiers of Axis A and Axis B frames, which are away from the bunker bay (Figure 2). Since the damping systems were uniformly added in Retrofit Design B, the reduction can be observed in both *X*-directional and *Y*-directional drift demands for most tiers. Recall that Retrofit Design C adopted isolations for coal bunkers along with added damping devices but less than those in Retrofit Design B. Its performance is in the middle of the other two retrofit designs in terms of the *X*-directional drift demands and the best in terms of the *Y*-directional drift demands.

The average of peak tier drift and residual tier drift over all considered intensities (i.e., 60% to 140% MCE) are shown in Figures 16a and 16b, respectively. It is clear from Figure 16a that the original design has the largest drift response among the four structures at each earthquake intensity. For the other three retrofit buildings, Retrofit Design B experienced the smallest drift response under 60% MCE intensity and followed by Retrofit Design C and Retrofit Design A. The peak tier drift is mainly determined by the results obtained from the first and fifth tiers of Axis D in *X* direction. Since there are no added damping devices distributed in first to fifth tiers of Axis D (Table 3), the peak tier drift of Retrofit Design C is

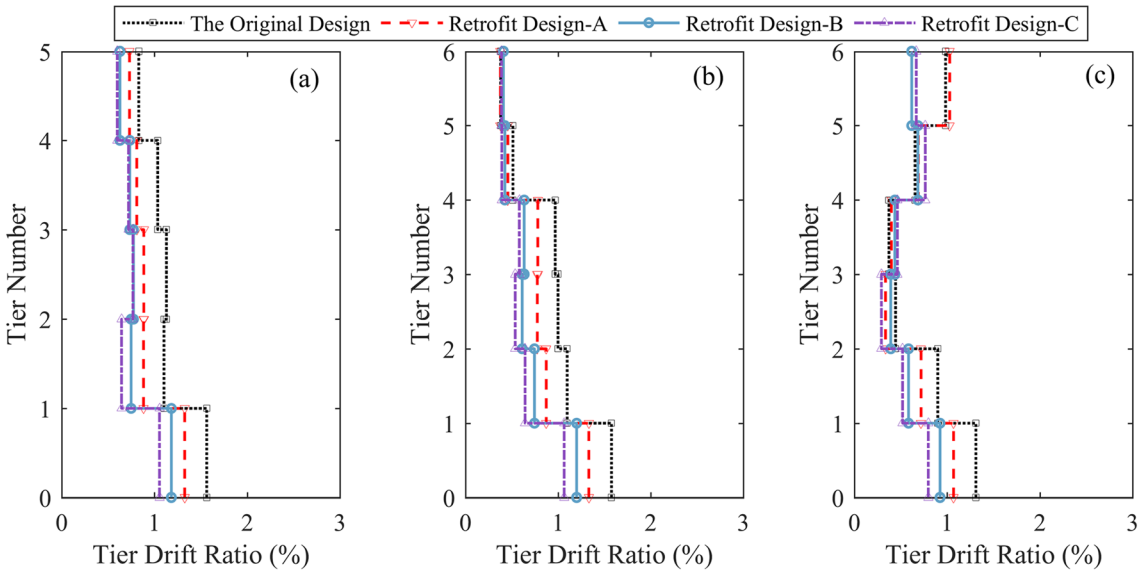


**FIGURE 15** Distributions of mean story drift ratios under 100% MCE in *Y* direction for columns in (a) Axis A, (b) Axis B, (c) Axis D

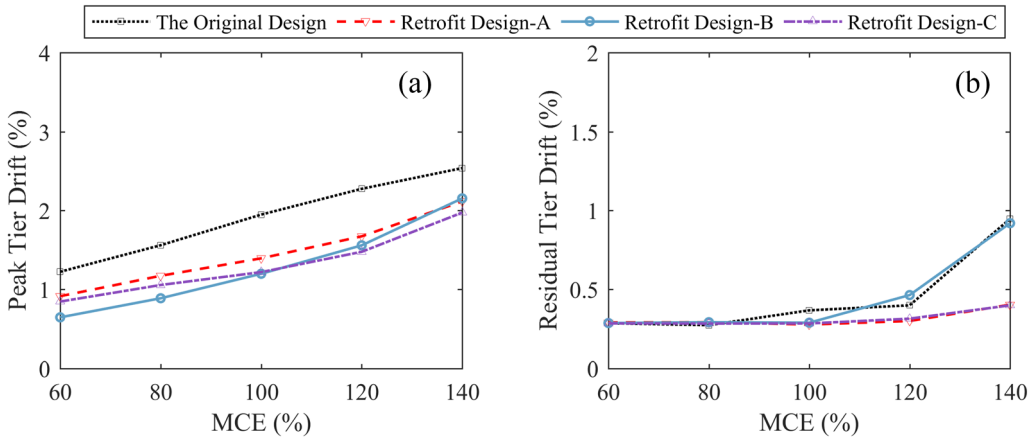


**FIGURE 16** Distribution profile of drift demands over 60–140% MCE intensities: (a) peak tier drift; (b) residual tier drift

slightly larger than the Retrofit Design B. With the increase of ground motion intensity level, the results of the three retrofit buildings are getting close and Retrofit Design B turns to be the one experienced the largest peak drift demand under the highest intensity level (i.e., 140% MCE). The result of residual drift distributions in Figure 16b shows a different trend. Under 60% and 80% MCE excitations, the residual drift values of all designs are close. When the excitation intensity increases to 100% MCE, the mean residual drift value of the original design goes up to 0.24% while the values of the rest structures are still below 0.2%. A significant increase in residual drift for the original design is observed when the excitation intensity is beyond 100% MCE, and it achieves at 0.9% at the end (i.e., 140% MCE). It is worth noting that Retrofit Design B has a sudden increase in residual drift response when the excitation intensity is greater than 100% MCE, which leads to a minimal difference from the results of the original design. On the contrary, the retrofit structures that employed isolation for coal bunkers (i.e., Retrofit Design A and Retrofit Design C) have smaller residual drift demands at the two highest excitation levels.

For the isolation layers of coal bunkers, the collisions between two adjacent coal bunkers and between coal bunkers and structural/-nonstructural components are not allowed. The peak and residual lateral displacements of the isolation layers along *X* and *Y* directions over the considered intensities are plotted in Figure 17. Recall that the maximum displacement limitations for the isolation layers are 385 mm along both *X* direction and *Y* direction (Figure 4). As seen in Figure 17, the maximum displacement in *Y* direction under the 140% MCE intensity is 335.9 and 328.3 mm for Retrofit Design A and Retrofit Design C, respectively. Also, the permanent displacements of the isolation layer are 17 and 13 mm under 140% MCE earthquake level for Retrofit Design A and Retrofit Design C, respectively, which are acceptable for immediate operation after earthquakes.

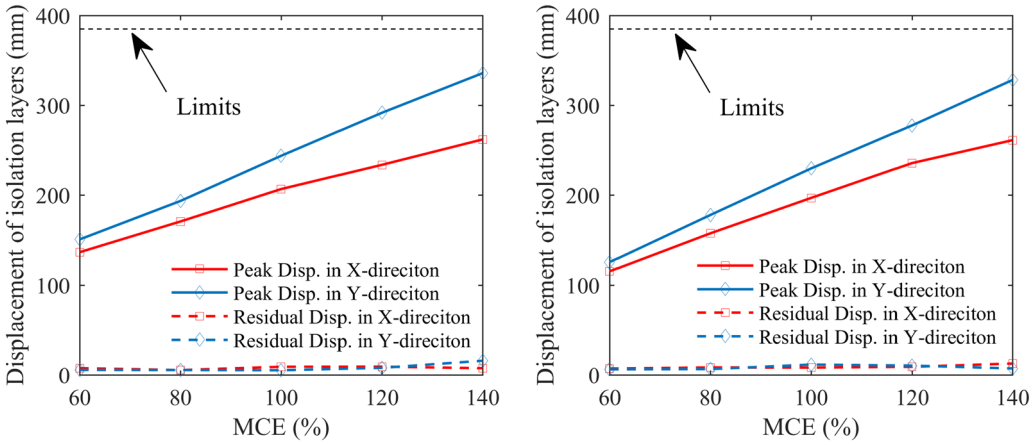


**FIGURE 17** Lateral displacement of isolation layers for coal bunkers

## 5.3 | Probabilistic seismic demand model development

To derive the seismic risk, the probabilistic seismic demand model (PSDM) is first built to link the engineering demand parameter (EDP) to the ground motion intensity measure (IM). A general mathematical formula of the seismic demand model can be expressed by Equation (1).[49] One of the most commonly used IMs is the spectral acceleration at the first-mode period, $S_a(T_1)$. However, as evidenced by the obtained modal analysis results, the seismic behaviors of the TPP building are not dominantly controlled by the first mode because of its highly structural complexity. Some researchers proposed some alternatives of IM such as PGA, PGV, Aerial Intensity (AI; e.g., Giovenale et al.[50]). In these prior studies, PGA is widely suggested as the primary IM to measure the vulnerability of complex industrial buildings.[51,52] Therefore, in the current study, PGA is used as the IM for the PSDM development. The peak tier story drift $\theta_{max}$ is considered as the EDP as it relates well to damage states as suggested by modern performance assessment guidelines or tools (e.g., ASCE/SEI 41-13,[44] Hazus-MH[53]). Based on the RHA results, a nonlinear regression analysis of the power-law form is performed to obtain the required parameters of $a$ and $b$ (Equation (1)) as well as the dispersion of the demand $\beta_{EDP|IM}$ (Equation (2)). An example of the regression model based on the analysis results of the original design can be seen in Figure 18. A comparison of the demand models among the three retrofit designs and the original design is made in Figure 19, and the associated demand parameters are listed in Table 6. It is observed that when PGA is less than 0.75 g, the $\theta_{max}$ of Retrofit Design B has the smallest value and afterwards, it exceeds the values of Retrofit Design C. Additionally, the Retrofit Design B has a larger dispersion (i.e., $\beta_{EDP|IM}$) than the other three models.

$$EDP = a \cdot IM^b \tag{1}$$

$$\beta_{EDP|IM} = \sqrt{\frac{\sum_{i=1}^{N}\left[\ln(EDP) - \ln\left(aIM^b\right)\right]^2}{N-2}} \tag{2}$$

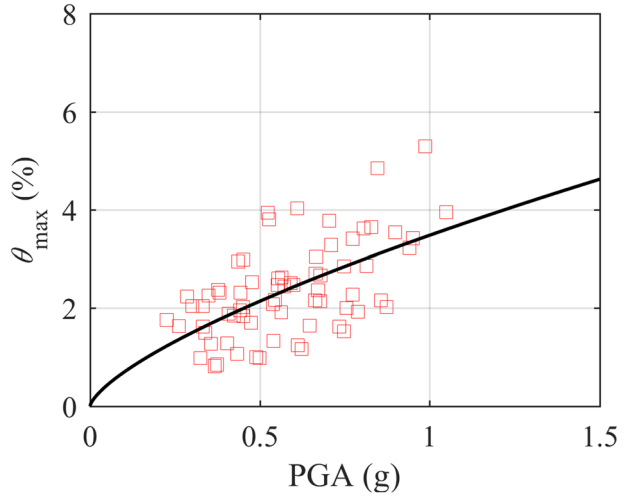


**FIGURE 18** Probabilistic seismic demand model of the original design

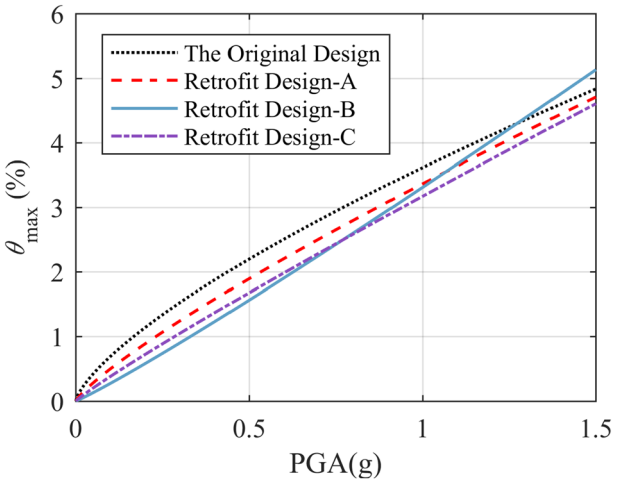


**FIGURE 19** Comparison of the PSDMs for the four designed structures

**TABLE 6** Parameter values of the PSDMs for the four designed structures

| Design scheme | a | b | β |
|---|---|---|---|
| Original design | 3.48 | 0.70 | 0.36 |
| Retrofit Design A | 3.23 | 0.82 | 0.37 |
| Retrofit Design B | 3.18 | 1.12 | 0.42 |
| Retrofit Design C | 2.99 | 0.89 | 0.39 |

where $N$ is the number to total simulation cases.

## 5.4 | Characterization of damage states and fragility development

The probability of exceeding a damage state on the condition of IM can be expressed by fragility curves. The damage states for the TPP building are defined, and each one represents a specific level of functionality. For SCBF systems, some popular performance-based guidelines such as the ASCE/SEI 41-13[44] and FEMA 356[54] have specified a series of discrete damage states, usually termed immediate occupancy (IO), life safety (LS), and collapse prevention (CP). The associate limit values for these damage states in terms of peak story drift are 0.5%, 1.5%, and 2%, respectively. Considering nonstructural components housed in the TPP building are different from residential buildings, three damages states that incorporate both structural components and industrial equipment are proposed as seen in Table 7.

A lognormal cumulative distribution function is used to model the seismic fragility which can be modeled as[55]:

**TABLE 7** Damage states considered for the TPP building

| Damage state | Structural elements | Nonstructural elements |
|---|---|---|
| DS1: Slight damage | Minor yielding or buckling of braces. Peak tier drift $\theta_{max}$ exceeds 0.5% | Turbine tripping, light damage to electric generators |
| DS2: Moderate damage | Many braces yield and buckle but do not totally fail. Many connections may fail. Peak tier drift $\theta_{max}$ exceeds 1.5% | Instrument panels and racks sliding, but no overturning; some realignment required to operate; considerable damage to pressure vessels or considerable damage to vertical pumps for deaerator and feedwater heater |
| DS3: Extensive damage | Extensive yielding and buckling of braces. Many braces and their connections may fail. Peak tier drift $\theta_{max}$ exceeds 2% | Extensive damage to large horizontal vessels beyond repair; extensive damage to anchored supports of large equipment such as deaerator and feedwater heater; Sensitive equipment such as generators and condensors being unfunctional; Some pipelines rupture. |

$$P[D > C|IM = x] = 1 - \Phi\left[\frac{\ln\left(\hat{C}/\hat{D}\right)}{\sqrt{\beta_{D|IM}^2 + \beta_C^2 + \beta_M^2}}\right] \tag{3}$$

where $\Phi[\cdot]$ is the standard normal probability integral; $\hat{C}$ is the median structural capacity associated with a certain limit state; $\hat{D}$ is the median seismic demands predicted by the PSDM; $\beta_M$ and $\beta_C$ represent the epistemic uncertainty in modeling and aleatoric uncertainty in seismic capacity ($C$), respectively.

The fragilities of all designed buildings for the considered three damage states (Table 7) are computed and compared in Figure 20. The capacity and epistemic uncertainties, $\beta_C$ and $\beta_M$ are both assumed as 0.2 as suggested by Ellingwood et al.[55] As seen in Figure 20a, the differences among the results of the four designs are minimal. The median capacity of the Retrofit Design B is 0.20 g while the original design has a median capacity of 0.06 g. The benefit of retrofit strategies becomes evident when it comes to the fragilities of DS2 and DS3. For example, the original design has the largest probability of exceedance for DS2 and DS3. The corresponding median capacities of the original design are 0.30 and 0.45 g for DS2 and DS3, respectively. Compared to these results, the median capacities of Retrofit Design A and Retrofit Design B are 33% and 87% larger than that of DS2; 13% and 47% larger than that of DS3, respectively. The fragility result of Retrofit Design C is comparable to Retrofit Design B especially for DS3.

## 5.5 | Seismic risk and restoration analysis

The mean annual probability of exceedance for a certain damage state can be used to describe the seismic risk, which is computed by:

$$\lambda_{DSi} = \int_0^\infty P(D > C_{DSi}|PGA = x) \cdot dH(x) \tag{4}$$

where $P(D > C_{DSi}|\ PGA = x)$ represents the probability of exceedance for a designated damage state when the $PGA$ value is equal to $x$; $H(x)$ is the seismic hazard function described by the mean annual frequency for an earthquake incident with the $PGA$ greater than $x$.

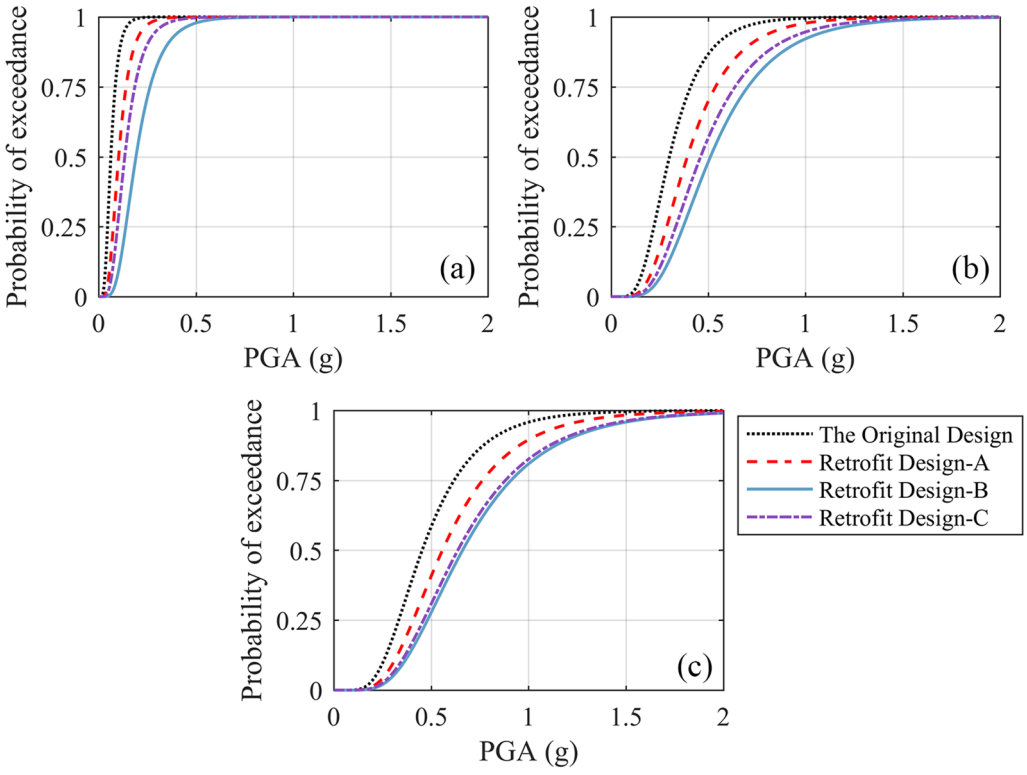


**FIGURE 20** Fragility curves of four designed structures for (a) DS1, (b) DS2, and (c) DS3

The site-specific seismic hazards (i.e., $H(x)$) where the actual TPP building is located are obtained with the help of MCPRC[56] and are plotted in Figure 21. The annual probability of exceedance in terms of $\theta_{max}$ for each design scheme is computed with Equation (4) and compared in Figure 22. Consistent with the observations from PSDMs, the Retrofit Design B has the smallest drift hazard, but it exceeds the results of Retrofit Design A and Retrofit Design C when $\theta_{max}$ = 2.4%. The drift hazards of the original design and Retrofit Design A are close when $\theta_{max}$ is less than 0.6%. Assuming that the occurrence of earthquakes follows a Poisson process,[57] the probability of exceeding the designated damage states over $t$ years can be computed by using Equation (5). The results for a period of 50 years are presented in Table 8. Compared to the probability of exceeding DS3 for the original design, the seismic risk is reduced at most by 27%, 45%, and 41% for Retrofit Design A, Retrofit Design B, and Retrofit Design C, respectively. The use of supplemental damping systems shows a greater benefit than the isolation of coal bunkers.

$$P(DSi \text{ in } t \text{ years}) = 1 - \exp(-\lambda_{DSi} t) \tag{5}$$

The development of the performance-based theory allows the stakeholders to participate in decision making together with professional engineers. Downtime is one of the frequently used measures to describe the consequences of earthquakes. For electric power generation system, Hazus-MH[53] provided empirical models to estimate the downtime or recovery time from seismic damage. The expected downtime conditioned

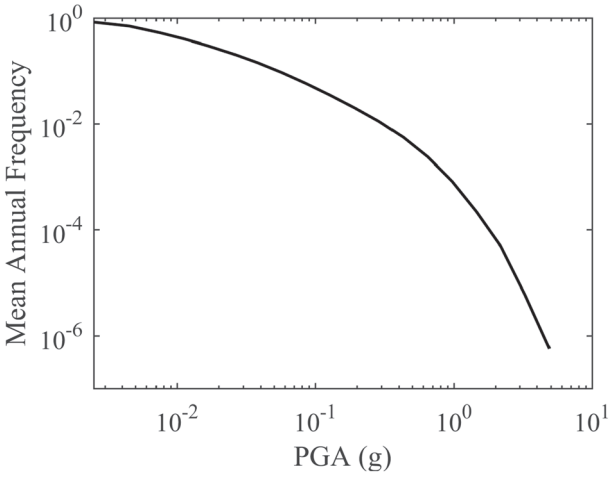


**FIGURE 21** Seismic hazard curve for the thermal power plant

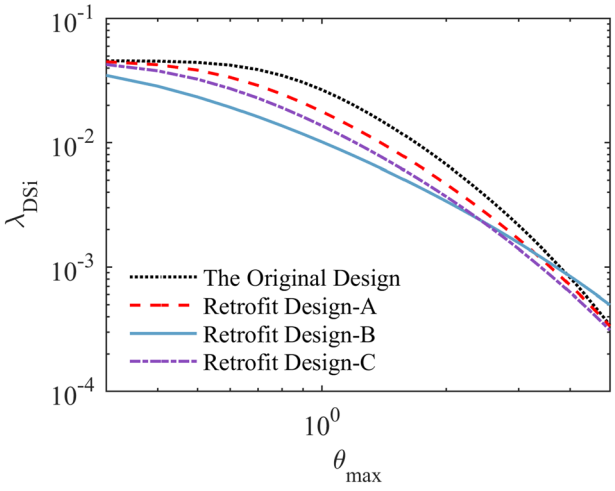


**FIGURE 22** Drift hazard levels for the four designs

**TABLE 8** Probability of exceeding damage states over 50 years for the four designs

| Damage state | Original design | Retrofit Design A | Retrofit Design B | Retrofit Design C |
|---|---|---|---|---|
| DS1 | 89.0% | 85.2% | 68.7% | 80.1% |
| DS2 | 47.5% | 34.9% | 24.0% | 28.3% |
| DS3 | 28.4% | 20.7% | 15.5% | 16.8% |

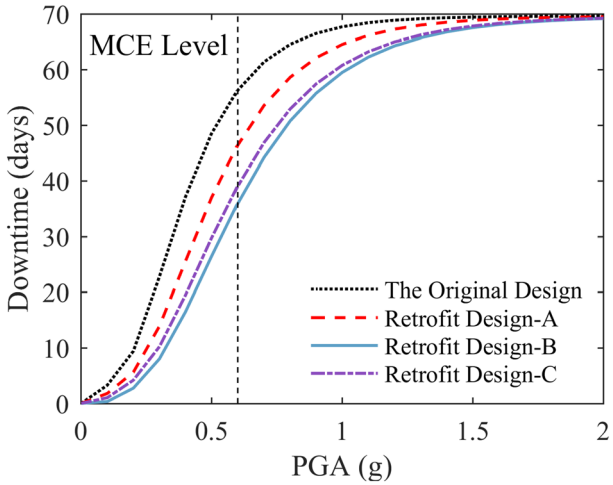


**FIGURE 23** Downtime estimation for different design schemes

on a specific IM can be evaluated by using Equation (6). With the obtained structural fragilities (Figure 20), the downtime over the variation of PGA values for four designs are compared in Figure 23. Take an earthquake incident at MCE intensity level (i.e., PGA = 0.6 g) as an example, the electric power restoration would cost 56, 49, 36, and 39 days for the original design, Retrofit Design A, Retrofit Design B, and Retrofit Design C, respectively. It is noted that different from the seismic risk results, Retrofit Design B and Retrofit Design C have nearly the same downtime. Similarly, considering the site-specific seismic hazard, in a period of 50 years the downtime for the four structures are 26, 20, 15, and 17 days. Compared to the original design, the reduction of downtime induced by different retrofit strategies are 23.1%, 42.3%, and 34.6% for Retrofit Design A, Retrofit Design B, and Retrofit Design C.

$$E(days|IM) = \sum_{i=1}^{i=3} E(days|DS_i)P(DS_i|IM) \tag{6}$$

## 6 | DISCUSSIONS AND RESEARCH SIGNIFICANCE

Based on the comparisons in seismic demands, the use of supplemental damping systems showed a better performance than others in terms of peak tier drift. However, it is noted that the Retrofit Design B has a comparable result with the original design for residual tier drift demands when the earthquake intensity is greater than 100% MCE level. This is partly due to the hysteretic properties of the metallic damping devices. This shortcoming regarding residual deformation left after earthquake was also a concern in plenty of studies (e.g., Erochko, 2011[58]; Deylami and Mahdavipour, 2015[59]; Kiggins & Uang, 2006[60]), and consequently, self-centering braces and innovative systems were proposed to eliminate the permanent deformation (e.g., Guan et al., 2018[61]; Tremblay et al., 2008[62]). In contrast, the Retrofit Design A and Retrofit Design C that have used isolation for coal bunkers experienced larger peak drift responses but left smaller residual drifts. Additionally, the residual displacement of the isolation layers is minimal enough for immediate operation even after an earthquake at 140% MCE level. When it comes to the structural damage quantified by peak drift demands, the associated repair costs for the Retrofit Design A and Retrofit Design C are likely larger than the Retrofit Design B. But extra costs related to the replacement of damping devices are inevitable for the Retrofit Design B. A detailed comparison in the aspect of detailed cost-benefit analysis is of interest in actual engineering projects.

Since economic loss is an important measure to describe the consequences caused by earthquakes, a nonstructural building model is needed together with the corresponding structural system. The nonstructural system housed in the TPP building includes a variety of components such as generators, turbines, racks, vessels, panels, and pipelines. In some modern performance-based guidelines, most stipulations associated with nonstructural elements are only applicable for residential and commercial buildings. The knowledge gap that lies in the seismic damage of industrial equipment warrants more efforts in the future. In this study, the seismic risk was assessed mainly in the aspect of the structural system. The damage states of some common industrial components are considered in this study (Table 7). However, it is a rough consideration. More detailed elaboration is required in further studies. If so, the retrofit system design would be performed based on the responses in both structural components and critical operational facilities. In addition, the interaction between coal material and the bunkers is not only normally ignored in seismic design as prescribed in guidelines[8,9] but also in prior studies in which similar silo-shape structures were focused.[23,63] Such issue is suggested to be studied in the future.

The industrial equipment housed in the TPP building are arranged in a typical way to serve to the physical power generation process. Therefore, the structural system is designed in a standard form like the building focused in this study. The proposed retrofit schemes and the seismic

risk assessment framework are expected to be explicitly refereed by practical professionals when doing similar engineering projects. Also, as presented in this study, the benefits in terms of seismic risk and downtime reduction from using damping and isolation techniques help stakeholders and social governors make thorough decisions regarding the retrofit strategy selection.

## 7 | CONCLUSIONS

Considering the essential role of the thermal power plant in an urban city, the performance of an actual TPP building retrofitted by different resilient strategies was assessed in this paper. The structural system of the TPP building is usually characterized by irregularities because of the operational constraints. To enhance its seismic performance, the isolation technique was employed to mitigate the detrimental effect of heavy coal bunkers. Also, the metallic low-point-yielding damping systems (i.e., YSPD and BRB) were considered as an alternative strategy. A total of three retrofit design schemes were proposed: Retrofit Design A used the isolation of coal bunkers only; Retrofit Design B used the added damping systems only; and Retrofit Design C used both isolation of coal bunkers and added damping systems. The performance of the original design that adopted SCBF as LFRS was taken as the baseline. The seismic demands of each designed structure were obtained from nonlinear RHAs. Subsequently, the benefit of each retrofit scheme was quantified in terms of seismic risk and downtime.

The seismic demands of structural frames along the two principal directions were compared. The peak drift profiles showed that the retrofit design schemes have smaller drift demands than the original design, especially for the critical tiers. The use of damping systems showed better performance than the isolation of coal bunkers in terms of peak tier drifts. However, under an earthquake intensity that beyond MCE, the performance of Retrofit Design B turned to be worse than the other two retrofit designs both in terms of peak tier drift and residual tier drift.

Based on the nonlinear RHA results, PSDMs and seismic fragilities corresponding to the proposed three damage states were developed. For Retrofit Design B, the predicted demands using PSDM were smaller than other design schemes when PGA is below 0.75 g. But Retrofit Design B has the largest dispersion in drift demands, which signifies the structural system with added damping devices is more susceptible to the record-to-record variety than the use of coal bunker isolations. The fragility results showed that the benefit of the considered retrofit strategies raises with the severity of structural damage states. Compared with the original design, the introduction of isolation for coal bunkers and added damping system increased the median seismic capacities at most by 29% and 62%. Convoluting the seismic fragilities with the site-specific hazard, the seismic risk results were obtained. The isolations for coal bunkers and added damping systems helped to mitigate the seismic risk by 19% and 38%, respectively. The seismic risk of the combined retrofit design scheme (i.e., Retrofit Design C) is comparable to that of Retrofit Design B. The downtime for all the considered design schemes were obtained and compared to reflect the benefit of different retrofit strategies in post-earthquake recovery. Retrofit Design B and Retrofit Design C have close results in downtime, which is approximately 20 days less than that of the original design if considering a single earthquake incident at the MCE intensity. Over a period of 50 years, the reductions of downtime are 23.1%, 42.3%, and 34.6% due to the use of isolation for coal bunkers, added damping system, and combined use of isolation and damping system, respectively.

Overall, for the TPP building considered in this study, the coal bunker isolation is less effective in the improvement of seismic performance and seismic risk than added damping systems. Under an earthquake event with an intensity greater than MCE level, the added damping systems failed to reduce the residual drift demands, which leads to a high likelihood of demolishment in the aftermath of the earthquake. The effectiveness of the combined use of isolation and damping system techniques is between the former two schemes. The selection of the retrofit strategies is suggested to be made based on the opinions of structural engineers, stakeholders, and professionals across other disciplines. This study could be profitably used as an example for further seismic risk evaluation for an industrial building equipped with resilient systems in practice.

### ACKNOWLEDGEMENTS

The authors would like to acknowledge China Scholarship Council, Power Construction Corporation of China through project KJ-2016-095, Program of Science and Technology Commission of Sichuan Province (18GJHZ0111), National Natural Science Foundation of China (U1710111 and 51878426), and Fundamental Research Funds for Central Universities of China to provide financial supports for the study.

### ORCID

*Kaoshan Dai* https://orcid.org/0000-0002-0193-6076

### REFERENCES

[1] S. Eshghi, M. S. Razzaghi, *Earthq. Spectra* **2005**, *21*, 395. https://doi.org/10.1193/1.2098810
[2] E. F. Cruz, D. Valdivia, *Struct Des Tall Spec Build* **2011**, *20*, 83. https://doi.org/10.1002/tal.679
[3] S. Fujita Seismic damage of mechanical structures by the 2011 Great East Japan Earthquake. 15th World Conf. Earthq. Eng., Lisbon,Portugal: **2012**.

[4] D. A. Bournas, P. Negro, F. F. Taucer, *Bull Earthq Eng* **2014**, *12*, 2383.
[5] E. Rossi, M. Ventrella, M. Faggella, R. Gigliotti, F. Braga, *ECCOMAS Congr 2016 - Proc 7th Eur Congr Comput Methods Appl Sci Eng* **2016**, *3*, 5. https://doi.org/10.7712/100016.2229.11993
[6] H. H. Erdem, A. V. Akkaya, B. Cetin, A. Dagdas, S. H. Sevilgen, B. Sahin, et al., *Int J Therm Sci* **2009**, *48*, 2179. https://doi.org/10.1016/j.ijthermalsci.2009.03.007
[7] World Coal Association. Coal and Electricity **2015**.
[8] ASCE, *ASCE 7-10 Minimum design loads for buildings and other structures*, American Society of Civil Engineers, Reston, VA **2010**.
[9] CEN. Eurocode 8: design of structures for earthquake resistance Part 1: general rules, seismic actions and rules for buildings (EN 1998-1). Brussels: European Committee of Standardization; **2013**.
[10] NCh. Earthquake Resistant Design of Industrial Structures and Facilities NCh 2369. Chilean Ministry of Housing; **2003**.
[11] B. R. Ellingwood, *Reliab Eng Syst Saf* **2001**, *74*, 251. https://doi.org/10.1016/S0951-8320(01)00105-3
[12] H. A. Rojas, C. Foley, S. Pezeshk, *Earthq. Spectra* **2011**, *27*, 857. https://doi.org/10.1193/1.3609877
[13] S. H. Hwang, D. G. Lignos, *Earthq Eng Struct Dyn* **2017**, *46*, 2141. https://doi.org/10.1002/eqe.2898
[14] C. M. Ramirez, E. Miranda, *Earthq Eng Struct Dyn* **2012**, *41*, 1477.
[15] D. Lu, X. Yu, M. Jia, G. Wang, *Struct Infrastruct Eng* **2013**, 1. https://doi.org/10.1080/15732479.2013.791326
[16] E. Tubaldi, M. Barbato, A. Dall'Asta, *Eng. Struct.* **2014**, *78*, 90. https://doi.org/10.1016/j.engstruct.2014.04.052
[17] M. R. Hossain, M. Ashraf, J. E. Padgett, *Eng. Struct.* **2013**, *56*, 1570. https://doi.org/10.1016/j.engstruct.2013.07.032
[18] E. Tafakori, M. Banazadeh, S. A. Jalali, M. Tehranizadeh, *Struct Des Tall Specail Build* **2013**, *22*, 700.
[19] A. B. Liel, G. G. Deierlein, *Earthq. Spectra* **2013**, *29*, 1391. https://doi.org/10.1193/030911EQS040M
[20] R. Han, Y. Li, J. van de Lindt, *Struct Saf* **2014**, *50*, 39. https://doi.org/10.1016/j.strusafe.2014.03.010
[21] J. I. Colombo, J. L. Almazán, *Eng. Struct.* **2015**, *98*, 201. https://doi.org/10.1016/j.engstruct.2015.04.037
[22] A. Kanyilmaz, C. A. Castiglioni, *Eng. Struct.* **2017**, *143*, 477. https://doi.org/10.1016/j.engstruct.2017.04.032
[23] M. Pinkawa, B. Hoffmeister, M. Feldmann. Performance Assessment of Seismic Retrofitting Measures on Silo Structures Using Innovative Seismic Protection Systems. Proc. VII Eur. Congr. Comput. Methods Appl. Sci. Eng. (ECCOMAS Congr. 2016), **2016**, p. 5851–67. doi:https://doi.org/10.7712/100016.2225.8876.
[24] F. Paolacci, R. Giannini, M. de Angelis, *J Loss Prev Process Ind* **2013**, *26*, 924. https://doi.org/10.1016/j.jlp.2013.03.003
[25] J. Wang, K. Dai, Y. Yin, S. Tesfamariam, *Eng. Struct.* **2018**, *164*, 141. https://doi.org/10.1016/j.engstruct.2018.03.001
[26] R. W. Chanand, Z. Zhao, *Appl. Mech. Mater.* **2012**, *238*, 833. https://doi.org/10.4028/www.scientific.net/AMM.238.833
[27] A. Wanitkorkul, A. Filiatrault, *Eng. Struct.* **2008**, *30*, 675. https://doi.org/10.1016/j.engstruct.2007.05.013
[28] E. Karamanci, D. G. Lignos, *J Struct Eng* **2014**, *140*, A4014019. https://doi.org/10.1061/(ASCE)ST.1943-541X.0001011
[29] R. Sabelli, S. Mahin, C. Chang, *Eng. Struct.* **2003**, *25*, 655. https://doi.org/10.1016/S0141-0296(02)00175-X
[30] R. W. K. Chan, F. Albermani, S. Kitipornchai, *J. Constr. Steel Res.* **2013**, *91*, 14. https://doi.org/10.1016/j.jcsr.2013.08.013
[31] E. Uckan, B. Akbas, J. Shen, R. Wen, K. Turandar, M. Erdik, *Nat. Hazards* **2015**, *75*, 265. https://doi.org/10.1007/s11069-014-1319-9
[32] B. V. Fell, A. M. Kanvinde, G. G. Deierlein, A. T. Myers, *J Struct Eng* **2009**, *135*, 19. https://doi.org/10.1061/(ASCE)0733-9445(2009)135:1(19)
[33] K. Dai, B. Li, J. Wang, A. Li, H. Li, J. Li, et al., *Struct Des Tall Spec Build* **2018**, *27*, e1477. https://doi.org/10.1002/tal.1477
[34] AISC, *AISC 360-10 Specifications for structural steel buildings. ANSI/AISC*, American Institute of Steel Construction, Chicago **2010**.
[35] AISC, *AISC 341-10 Seismic provisions for structural steel buildings. ANSI/AISC*, American Institute of Steel Construction, Chicago **2010**.
[36] D. E. Lehman, C. W. Roeder, D. Herman, S. Johnson, B. Kotulka, *J Struct Eng* **2008**, *134*, 890. https://doi.org/10.1061/(ASCE)0733-9445(2008)134:6(890)
[37] L. Hao, R. Zhang, K. Jin, *Earthq Eng Struct Dyn* **2018**, *47*, 515. https://doi.org/10.1002/eqe.2977
[38] CSI. SAP2000 Version 18. Optimized Modeling and Design of Structures Using SAP2000. **2015**.
[39] A. Asghari, A. H. Gandomi, *Struct Infrastruct Eng* **2016**, *12*, 239. https://doi.org/10.1080/15732479.2015.1009123
[40] T. Balendra, M.-T. Sam, C.-Y. Liaw, S.-L. Lee, *Eng. Struct.* **1991**, *13*, 67.
[41] E. Junda, S. Leelataviwat, P. Doung, *J. Constr. Steel Res.* **2018**, *148*, 154. https://doi.org/10.1016/j.jcsr.2018.05.012
[42] S. Leelataviwat, B. Suksan, J. Srechai, P. Warnitchai, *J Struct Eng* **2011**, *137*, 579. https://doi.org/10.1061/(ASCE)ST.1943-541X.0000301
[43] CSI. Nonlinear analysis and performance assessment for 3D structures **2013**.
[44] ASCE, *Seismic Evaluation and Retrofit of Existing Buildings ASCE/SEI 41-13*, American Society of Civil Engineers, Reston, VA **2014**.
[45] J. Powell, *Evaluation of special concentrically braced frames for improved seismic performance and constructability (Master thesis)*, University of Washington, Seattle, WA, USA **2010**.
[46] K. Liu, K. Dai, A. Li, H. Li, J. Wang, B. Li. Shaking table test model design of a large complex power plant structure. 264th China Eng. Sci. Technol. Forum 10th Natl. Conf. Earthq. Disaster Prev. Mitig. Eng., Chengdu, China: **2018**.
[47] M. S. Speicher, J. L. Harris, *Eng. Struct.* **2018**, *164*, 274. https://doi.org/10.1016/j.engstruct.2018.01.067
[48] PEER. Pacific Earthquake Engineering Research Center PEER Ground Motion Database **2018**. http://ngawest2.berkeley.edu/.
[49] C. A. Cornell, F. Jalayer, R. O. Hamburger, D. A. Foutch, *J Struct Eng* **2002**, *128*, 526. https://doi.org/10.1061/(ASCE)0733-9445(2002)128:4(526)
[50] P. Giovenale, M. Ciampoli, F. Jalayer. Comparison of ground motion intensity measures using the incremental dynamic analysis. In: Kiureghian D, editor. Appl. Stat. Probab. Civ. Eng., Madanat & Pestana (eds); **2003**.
[51] A. Panico, A. Basco, G. Lanzano, F. Pirozzi, F. Santucci de Magistris, G. Fabbrocino, et al., *Saf Sci* **2017**, *97*, 51. https://doi.org/10.1016/j.ssci.2015.12.030
[52] E. Salzano, A. Garcia Agreda, A. Di Carluccio, G. Fabbrocino, *Reliab Eng Syst Saf* **2009**, *94*, 1577. https://doi.org/10.1016/j.ress.2009.02.023
[53] Hazus. Hazus–MH 2.1: Technical Manual. **2012**.
[54] FEMA, *Prestandard and commentray for the seismic rehabilitation of buildings*, Federal Emergency Management Agency, Washington, DC **2000**.
[55] B. R. Ellingwood, O. C. Celik, K. Kinali, *Earthq Eng Struct Dyn* **2007**, *36*, 1935. https://doi.org/10.1002/eqe.693
[56] MCPRC, *Seismic ground motion parameters zonation map of China*, Ministry of Construction of Peoples Republic of China, Beijing, China **2015**.
[57] C. A. Cornell, *Bull. Seismol. Soc. Am.* **1968**, *58*, 1583.
[58] J. Erochko, C. Christopoulos, R. Tremblay, H. Choi, *J Struct Eng* **2011**, *137*, 589. https://doi.org/10.1061/(ASCE)ST.1943-541X.0000296

[59] A. Deylami, M. A. Mahdavipour, *Struct Saf* **2016**, *58*, 31. https://doi.org/10.1016/j.strusafe.2015.08.004
[60] S. Kiggins, C. M. Uang, *Eng. Struct.* **2006**, *28*, 1525. https://doi.org/10.1016/j.engstruct.2005.10.023
[61] X. Guan, H. Burton, S. Moradi, *J. Constr. Steel Res.* **2018**, *150*, 129. https://doi.org/10.1016/j.jcsr.2018.07.026
[62] R. Tremblay, M. Lacerte, C. Christopoulos, *J Struct Eng* **2008**, *134*, 108. https://doi.org/10.1061/(ASCE)0733-9445(2008)134:1(108)
[63] R. J. Merino Vela, E. Brunesi, R. Nascimbene, *Eng. Struct.* **2018**, *171*, 105. https://doi.org/10.1016/j.engstruct.2018.05.053

**How to cite this article:** Wang J, Dai K, Li B, et al. Seismic retrofit design and risk assessment of an irregular thermal power plant building. *Struct Design Tall Spec Build.* 2020;29:e1719. https://doi.org/10.1002/tal.1719